第 43 卷 第 5 期/2023 年 3 月/光学学报 研究论文

光学学报

# 脉冲叠加技术提升脉冲展宽分幅相机时间均匀性

伍思其[1]，白雁力[1]，高海英[2*]，姚荣彬[2]，刘达见[2]

[1]桂林电子科技大学电子工程与自动化学院，广西 桂林 541004；

[2]桂林电子科技大学信息与通信学院，广西 桂林 541004

**摘要** 脉冲展宽分幅相机是时间分辨率优于10 ps的二维超快诊断设备，但展宽脉冲沿阴极传输会引起阴极不同位置的电压分布出现差异，这会导致相机时间不均匀现象的产生，从而限制了大探测面相机的实现。采用雪崩三极管、雪崩二极管和高通滤波器设计了一种快斜率皮秒选通脉冲，基于电脉冲叠加原理，探讨了选通脉冲下降沿对时间不均匀性的提升效果。研究结果显示：当阴极电压为－2 kV、电子束初始时间宽度为5 ps和展宽斜率为11.9 V/ps时，随着展宽脉冲沿阴极起点传输到终点，阴极上的电子束展宽倍率由11.74增至39.04，基于相对误差原理，两者相差232.5%；当将选通脉冲下降沿和展宽脉冲同时加载至阴极时，电子束展宽倍率由11.28变化至14.23，两者相差下降至40.21%，此时脉冲展宽分幅相机的时间分辨均匀性得到了有效提升。

**关键词** 超快光学；超快诊断技术；脉冲展宽分幅相机；脉冲叠加技术；时间均匀性

**中图分类号** TN143 **文献标志码** A **DOI**：10.3788/AOS221488

## 1 引 言

在惯性约束聚变(ICF)实验中，分幅相机是有效记录等离子体瞬态过程的二维超快诊断设备[1-2]。目前，主流分幅相机包括微通道板式(MCP)和脉冲展宽式[3]。在行波选通MCP分幅相机中，受到光电子的渡越时间及其时间弥散的影响，时间分辨率被局限于60～100 ps范围内[4]，虽然将MCP的厚度减小到0.2 mm，可将时间分辨率提升至约35 ps[5]，但是薄MCP存在信噪比差、制作工艺复杂的缺点，故难以获得广泛应用。为了进一步提升时间分辨率，研究者将脉冲展宽技术、磁聚焦技术和MCP分幅相机相结合，研制出了时间分辨率优于10 ps的脉冲展宽分幅相机[6-10]，该相机包括加速区、漂移区和成像区三部分：在加速区中，通过加载时变电场使电子束前沿具有更大的加速能量；在漂移区中，通过长距离传输使电子束时间宽度展宽；在成像区中，采用MCP分幅相机测量展宽后的电子束信号，获得了成倍提升的时间分辨率。随着ICF实验对更快时间分辨超快诊断设备的需求，脉冲展宽分幅相机逐渐成为该领域的研究热点。

脉冲展宽分幅相机的时间分辨率与加速电压、展宽脉冲斜率、漂移区长度和MCP分幅相机的时间分辨率相关[11-13]，其中漂移区长度和MCP分幅相机的时间分辨率通常取固定参数。为便于展宽脉冲传输，相机加速区中的阴极采用微带结构设计，当展宽脉冲加载于阴极时，由于展宽脉冲会沿阴极传输，故根据电脉冲叠加原理，阴极电压会随着展宽脉冲上升沿的幅值而发生变化，从而造成阴极上不同位置具有不同的电子束展宽倍率和时间分辨率，即脉冲展宽分幅相机的时间不均匀性，这是制约该相机向大探测面方向发展的主要因素之一[14]。

为克服脉冲展宽分幅相机时间不均匀性的制约，设计了一种皮秒选通脉冲，基于展宽脉冲沿阴极传输的电压变化特性，将选通脉冲下降沿和展宽脉冲同时加载于阴极上，对该方式提升时间均匀性的效果展开了研究。首先，介绍了脉冲展宽分幅相机的时间展宽倍率的计算方法和时间不均匀性的产生原理。然后，基于Marx电路和皮秒脉冲成形电路设计皮秒选通脉冲，并分析脉冲上升沿对脉冲展宽分幅相机时间不均匀性的影响。最后，基于电脉冲叠加原理，采用选通脉冲下降沿对时间均匀性进行提升。

## 2 脉冲展宽分幅相机时间不均匀性的产生原因

脉冲展宽分幅相机展宽倍率的计算原理如图1所示，包括展宽脉冲、加速区(阴极和阳极)、漂移区和成

**收稿日期**：2022-07-18；**修回日期**：2022-09-20；**录用日期**：2022-10-08；**网络首发日期**：2022-10-18

**基金项目**：国家自然科学基金(11865007)、广西自然科学基金面上项目(2022GXNSFAA035561)、广西自动检测技术与仪器重点实验室主任基金(YQ22101)

**通信作者**：*835960200@qq.com

像区(MCP分幅相机),其中展宽脉冲的上升斜率为$\alpha$(单位为V/ps),起点和终点的幅值分别为$\Phi_a$和$\Phi_b$(单位为V)。根据展宽脉冲沿阴极传输的特性,阴极起点$a$和终点$b$处产生的电子束,分别与展宽脉冲上升沿起点(幅值$\Phi_a$处)和终点(幅值$\Phi_b$处)的时间同步。在固定漂移区的情况下,$a$处和$b$处产生的电子束到达MCP处的展宽倍率为

$$M_a=1+\left(\frac{L}{\sqrt{2|-\Phi+\Phi_a+\alpha W_p|\eta}}-\frac{L}{\sqrt{2|-\Phi+\Phi_a|\eta}}\right)\Big/W_p, \tag{1}$$

$$M_b=1+\left(\frac{L}{\sqrt{2|-\Phi+\Phi_b+\alpha W_p|\eta}}-\frac{L}{\sqrt{2|-\Phi+\Phi_b|\eta}}\right)\Big/W_p \tag{2}$$

式中:$L$为漂移区长度;$W_p$为电子束的初始时间宽度;$\eta$为电子的荷质比;$-\Phi$为加载在阴极上的电压。由于$\Phi_a$和$\Phi_b$数值不同,因此随着展宽脉冲沿阴极传输,脉冲展宽分幅相机中的电子束展宽倍率和时间不均匀性随之产生。

根据电脉冲沿阴极的传输速度$v$为0.279 mm/ps[15],阴极上不同位置的展宽倍率$M_i$为

$$M_i=1+\left(\frac{L}{\sqrt{2|-\Phi+\Phi_i+\alpha W_p|\eta}}-\frac{L}{\sqrt{2|-\Phi+\Phi_i|\eta}}\right)\Big/W_p, \tag{3}$$

$$\Phi_i=\frac{d_i}{v}\alpha, \tag{4}$$

式中:$\Phi_i$为展宽脉冲传输到阴极$i$位置时的幅值;$d_i$为展宽脉冲沿阴极的传输距离。

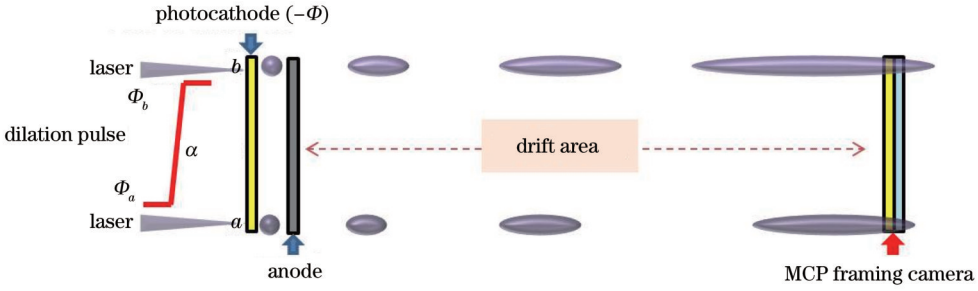


图1　脉冲展宽分幅相机展宽倍率计算原理

Fig. 1　Calculation principle of dilating ratio of pulse-dilation framing camera

## 3　皮秒选通脉冲设计

皮秒选通脉冲的设计如图2(a)所示,系统包括触发电路、三级Marx脉冲发生器和皮秒脉冲成形电路三部分:触发电路由方波触发信号源(Trig in)、触发电容$C_4$和触发电阻$R_7$~$R_9$构成;Marx脉冲发生器由直流电源HV、限流电阻$R_1$~$R_6$、雪崩三极管$Q_1$~$Q_{12}$和充电电容$C_1$~$C_3$构成,其中雪崩三极管采用串联和并联相结合的设计方式;皮秒脉冲成形电路由限流与滤波电感$L_1$和$L_2$、输出与滤波电容$C_7$和$C_8$、雪崩二极管$D_1$和$D_2$,以及负载电阻R组成。当系统工作时,先利用触发信号触发雪崩三极管$Q_1$,$Q_1$雪崩导通后系统运行状态由“高压低流”立即转变为“低压高流”,此时电流能够流过整个环路,而当电流增大到一定程度时,所有雪崩三极管将被二次击穿,此时Marx电路可输出纳秒超快阶跃高压脉冲。然后,将该脉冲作为皮秒脉冲成形电路的驱动源,脉冲经过具有隔离作用的限流电感$L_1$到达输出电容$C_7$,电容电压的上升会促使雪崩二极管$D_1$和$D_2$反向加压,当输入脉冲到达一定幅度时,二极管雪崩击穿,产生具有极快上升沿和下降沿的皮秒超快阶跃高压脉冲。最后,该脉冲经过电感$L_2$与电容$C_8$组成的高通滤波器后,可获得高幅值、窄半峰全宽的皮秒选通脉冲[16]。当直流电源HV的电压为1.92 kV,触发信号的幅值为5 V和频率为10 Hz,$R_1$~$R_{16}$为150 kΩ,$Q_1$~$Q_{12}$的型号为2N5551,$C_1$~$C_3$为2.3 nF,$C_4$~$C_6$为10 μF,$R_7$~$R_9$为100 Ω,$L_1$和$L_2$分别为725 nH和7 nH,$C_7$和$C_8$分别为2 pF和1 pF,$D_1$和$D_2$的型号为IN5408,输出负载R为50 Ω时,获得的皮秒选通脉冲如图2(b)所示,其幅值为−2.59 kV,半峰全宽为236 ps,上升沿和下降沿分别为217 ps和204 ps。

## 4　脉冲叠加技术提升脉冲展宽分幅相机时间均匀性

选通脉冲上升沿部分如图3(a)所示,脉冲上升沿

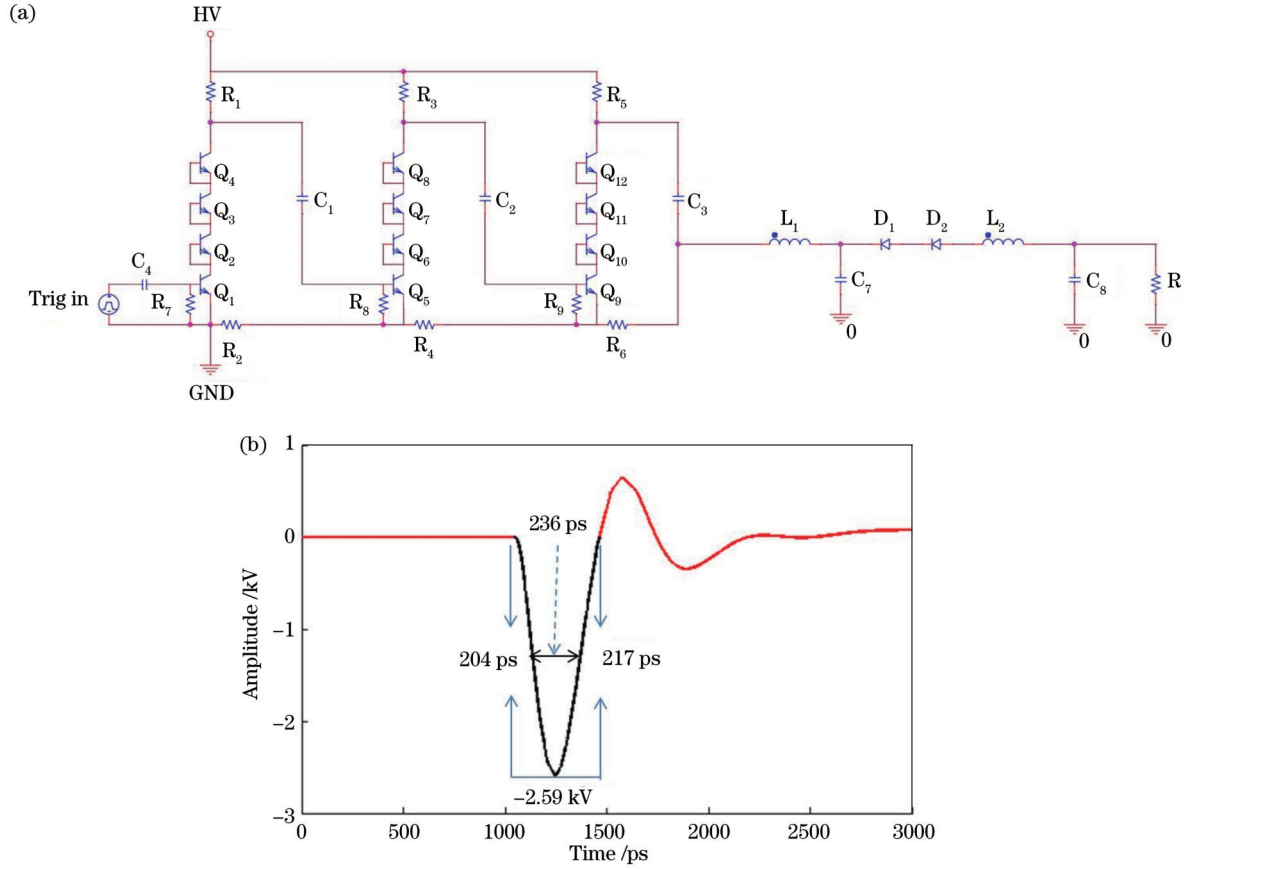


图 2　皮秒选通脉冲设计。(a)电路示意图;(b)输出的选通脉冲

Fig. 2　Design of picosecond gating pulse. (a) Schematic diagram of circuit; (b) output gating pulse

起点和终点的时刻分别为 1248 ps 和 1465 ps(即上升沿为 217 ps),幅值分别为 −2.59 kV 和 $-2.64\times10^{-3}$ kV,上升斜率 $\alpha$ 约为 11.9 V/ps。假设脉冲展宽分幅相机的阴极长度为 60 mm,电子束初始时间宽度为 5 ps,阴极加载初始电压 $-\Phi$ 为 −2 kV,漂移区长度 $L$ 为 0.5 m,根据式(3),阴极上不同位置的展宽倍率如图 3(b)所示。可以发现:当展宽脉冲上升沿起点与阴极起始端产生的电子束同步时,电子束展宽倍率为 11.74;随着展宽脉冲沿阴极传输,当展宽脉冲上升沿终端与阴极末端产生的电子束同步时,电子束展宽倍率为 39.04,基于相对误差原理,阴极两端的展宽倍率相差 232.5%,相应的计算公式为

$$\gamma_i=\frac{M_i-M_1}{M_1}\times100\%。\tag{5}$$

分析结果表明,随着展宽脉冲沿阴极传输,阴极上不同位置处产生的电子束将与展宽脉冲上升沿的不同位置同步,故展宽脉冲上升沿幅值的变化将会引起阴极上不同位置的电压出现差异,最终导致展宽倍率不均匀性现象产生。

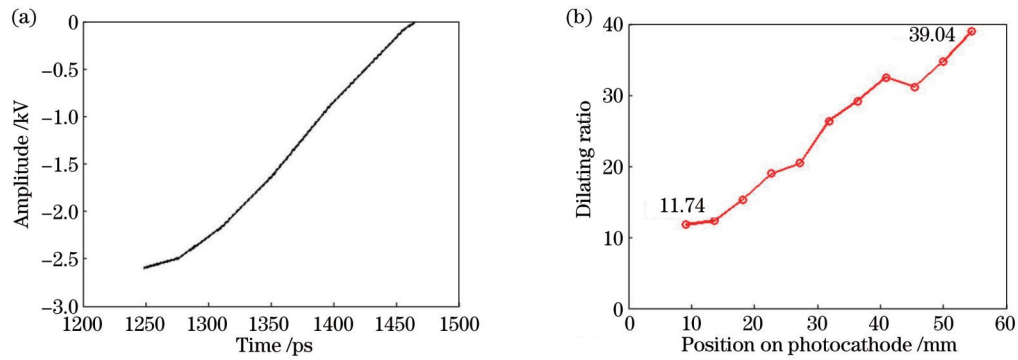


图 3　展宽脉冲沿阴极传输对展宽倍率的影响。(a)幅值随时间的变化曲线;(b)阴极不同位置处的展宽倍率

Fig. 3　Influence of dilating pulse transmission along photocathode on dilating ratio. (a) Amplitude varying with time; (b) dilating ratios at different photocathode positions

为降低展宽脉冲沿阴极传输对时间不均匀性的影响，在阴极上加载选通脉冲下降沿，基于脉冲叠加技术，优化阴极的电压分布。选通脉冲下降沿如图 4(a)所示，脉冲下降沿起点和终点的时刻分别为 1044 ps 和 1248 ps(即下降沿为 204 ps)，幅值分别为 $-1.12\times10^{-3}$ kV 和 −2.59 kV，下降斜率约为 12.7 V/ps。当将选通脉冲下降沿和展宽脉冲同时加载至阴极时，随着脉冲沿阴极传输，阴极上电压的分布情况如图 4(b)所示：当未加载下降沿脉冲时，阴极上不同采样点的电压由 −4.48 kV 变化至 −2.47 kV；在加载下降沿脉冲后，电压分布由 −4.62 kV 变化至 −4.97 kV，变化趋势明显平缓。根据式(3)计算展宽倍率，所得结果对比如图 4(c)所示，在加载下降沿脉冲后，展宽倍率由第 1 个采样点的 11.28 平缓变化到最后一个采样点的 14.23。根据式(5)的相对误差原理，其他采样点与第 1 个采样点的展宽倍率差值百分比如图 4(d)所示，加载下降沿脉冲后的展宽倍率变化过程明显平缓，阴极两端的展宽倍率相差下降至 40.21%，相较于未加载下降沿脉冲，时间均匀性得到了有效提升。

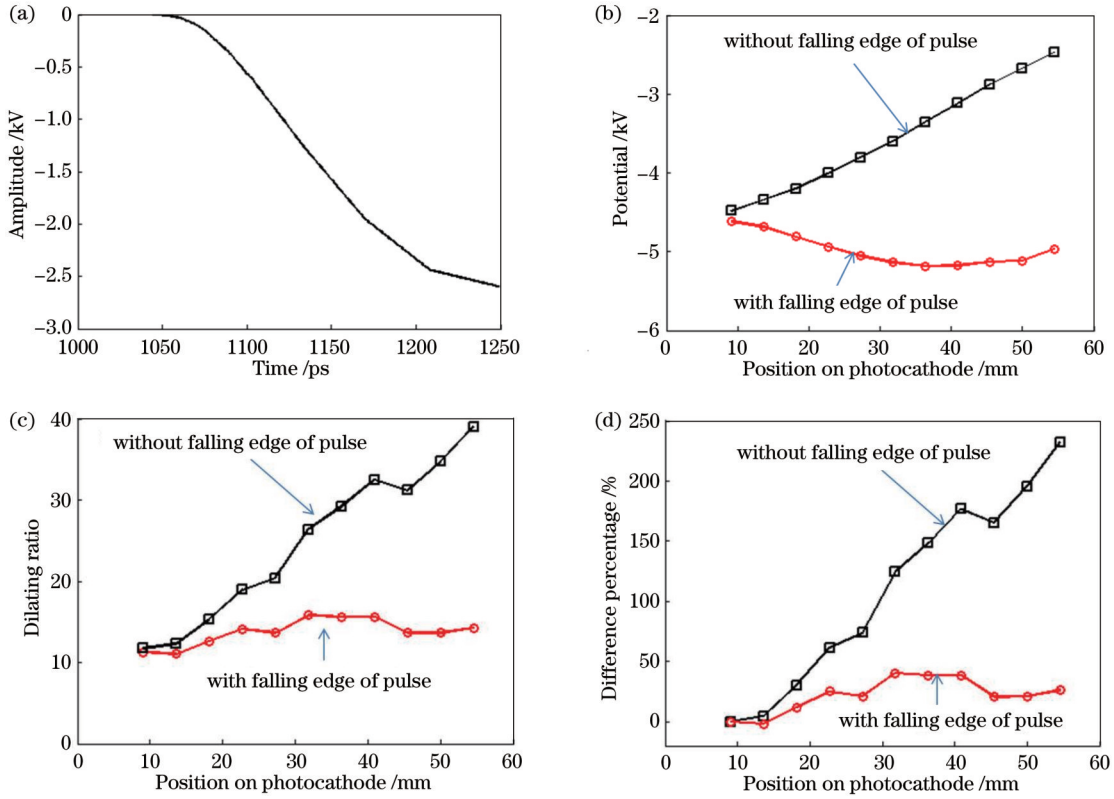


图 4　加载下降沿脉冲对时间不均匀性的影响。(a)下降沿脉冲；(b)沿阴极的电压变化对比；(c)沿阴极的展宽倍率对比；(d)其他采样点相对于第 1 个采样点的展宽倍率差值百分比

Fig. 4　Effect of falling edge of gating pulse on temporal uniformity. (a) Falling edge of pulse; (b) comparison of potential changes along photocathode; (c) comparison of dilating ratios along photocathode; (d) difference percentage of dilating ratio between other sampling points and first sampling point

## 5　结　　论

介绍了脉冲展宽分幅相机的工作原理、展宽倍率计算方法和时间不均匀性的产生原因，采用雪崩三极管串并联结构设计 Marx 脉冲发生器，采用雪崩二极管和高通滤波器设计皮秒选通脉冲成形电路。基于脉冲叠加技术，将选通脉冲的下降沿应用于脉冲展宽分幅相机的时间均匀性提升研究。研究结果表明，当阴极电压为 −2 kV、电子束初始时间宽度为 5 ps 和展宽脉冲上升斜率为 11.9 V/ps 时，随着展宽脉冲沿阴极传输，沿阴极的电压由 −4.48 kV 变化至 −2.47 kV，电子束展宽倍率由 11.74 增加至 39.04，基于相对误差原理，两者相差 232.5%。在此基础上，当在阴极上同时加载斜率为 12.7 V/ps 的下降沿脉冲时，沿阴极的电压由 −4.62 kV 变化至 −4.97 kV，电子束展宽倍率由 11.28 平缓地变化至 14.23，两者相差降低至 40.21%，时间均匀性得到显著提升。研究结论为提升脉冲展宽分幅相机时间不均匀性提供了一种有效的方法，为 10 ps 大探测面积分幅相机的研制提供了理论参考。

### 参　考　文　献

[1] Benedetti L R, Holder J P, Perkins M, et al. Advances in X-ray framing cameras at the National Ignition Facility to improve quantitative precision in X-ray imaging[J]. Review of Scientific Instruments, 2016, 87(2): 023511.

[2] Zylstra A B, Hurricane O A, Callahan D A, et al. Burning plasma achieved in inertial fusion[J]. Nature, 2022, 601(7894): 542-548.
[3] Nagel S R, Benedetti L R, Bradley D K, et al. Comparison of implosion core metrics: a 10 ps dilation X-ray imager vs a 100 ps gated microchannel plate[J]. Review of Scientific Instruments, 2016, 87(11): 11E311.
[4] Khan S F, Spears B, Pak A, et al. Tracking the movement of the ICF hot spot using the time variance of the shape measured with gated X-ray cameras at NIF[J]. Meccanica, 2013, 48(3): 681-697.
[5] Bell P, Kilkenny J, Hanks R, et al. Measurements with a 35-psec gate time microchannel plate camera[J]. Proceedings of SPIE, 1990, 1346: 456-464.
[6] Hilsabeck T J, Hares J D, Kilkenny J D, et al. Pulse-dilation enhanced gated optical imager with 5 ps resolution (invited)[J]. Review of Scientific Instruments, 2010, 81(10): 10E317.
[7] Bai Y L, Long J H, Liu J Y, et al. Demonstration of 11-ps exposure time of a framing camera using pulse-dilation technology and a magnetic lens[J]. Optical Engineering, 2015, 54(12): 124103.
[8] 雷云飞, 刘进元, 蔡厚智, 等. 脉冲展宽分幅变像管场曲特性研究[J]. 光学学报, 2021, 41(21): 2132001.
Lei Y F, Liu J Y, Cai H Z, et al. Study on field curvature characteristics of pulse-dilation framing tube[J]. Acta Optica Sinica, 2021, 41(21): 2132001.
[9] 雷云飞, 刘进元, 蔡厚智, 等. 双透镜脉冲展宽分幅相机成像特性研究[J]. 激光与光电子学进展, 2022, 59(18): 1832001.
Lei Y F, Liu J Y, Cai H Z, et al. Imaging performance of double-lens pulse-dilation framing camera[J]. Laser & Optoelectronics Progress, 2022, 59(18): 1832001.
[10] 陈欢, 白雁力, 钟思. 脉冲展宽分幅变像管的最优成像磁场研究[J]. 激光与光电子学进展, 2022, 59(18): 1811007.
Chen H, Bai Y L, Zhong S. Optimal imaging magnetic field of pulse-dilation framing image converter tube[J]. Laser & Optoelectronics Progress, 2022, 59(18): 1811007.
[11] Nagel S R, Hilsabeck T J, Bell P M, et al. Dilation X-ray imager a new/faster gated X-ray imager for the NIF[J]. Review of Scientific Instruments, 2012, 83(10): 10E116.
[12] Bai Y L, Yao R B, Gao H Y, et al. Measurement of dilation pulses using a pulse-dilation framing camera[J]. Optics Express, 2020, 28(10): 15407-15415.
[13] Bai Y L, Yao R B, Gao H Y, et al. Measurement and analysis of temporal performance using different gradients of dilation pulse in the framing camera[J]. Optik, 2020, 221: 165360.
[14] Cai H Z, Fu W Y, Wang D, et al. Dilation X-ray framing camera and its temporal resolution uniformity[J]. Optics Express, 2019, 27(3): 2817-2827.
[15] Nagel S R, Hilsabeck T J, Bell P M, et al. Investigating high speed phenomena in laser plasma interactions using dilation X-ray imager (invited)[J]. Review of Scientific Instruments, 2014, 85(11): 11E504.
[16] Liu J Y, Niu L H, Peng W D, et al. Application of a fast electrical pulse in gated multichannel plate camera[J]. Review of Scientific Instruments, 2007, 78(5): 055104.

# Improvement of Temporal Uniformity of Pulse-Dilation Framing Camera Using Pulse Superposition Technique

Wu Siqi[1], Bai Yanli[1], Gao Haiying[2*], Yao Rongbin[2], Liu Dajian[2]

[1]*School of Electronic Engineering and Automation, Guilin University of Electronic Technology, Guilin* 541004, *Guangxi, China*;

[2]*School of Information and Communication, Guilin University of Electronic Technology, Guilin* 541004, *Guangxi, China*

## Abstract

**Objective** The framing camera is a two-dimensional (2D) ultrafast diagnostic device with high spatio-temporal resolution. In inertial confinement fusion (ICF) experiments, it can effectively acquire the duration and dynamic images at the stage of implosion compression. The pulse dilation framing camera is a new ultrafast diagnostic device with temporal resolution better than 10 ps. Firstly, this paper loads the dilating pulse between the photocathode (PC) and grid to achieve greater acceleration energy of the front edge of electron beams. Then, the temporal width of the electron beam is dilated through long-distance transmission. Finally, the dilated electron beam signal is measured by the microchannel plate (MCP) framing camera, and the temporal resolution is exponentially improved. However, in the pulse-dilation framing camera, with the transmission of dilating pulse along the PC, the voltage at different positions on the PC is changed, which results in temporal non-uniformity. This is one of the main factors restricting the development of framing cameras with large detection areas. To improve the restriction of temporal non-uniformity of the pulse-dilation framing camera, the gating pulse with picoseconds is designed, and the improvement of the temporal uniformity is studied by simultaneously loading the falling edge of the gating pulse and dilating pulse on the PC, which is based on the variational phenomenon of voltage during the transmission of dilating pulse along the PC.

**Methods** This paper first deduces the computational equation of the dynamic dilating ratio of the electron beam along the PC by analyzing the causes of temporal non-uniformity and combines the principle of temporal dilation and the transmission

characteristics of the electric pulse along the PC. Then, the high-voltage gating pulse with picoseconds is designed by the three-stage Marx pulse generator and the pulse shaping circuit. The Marx pulse generator is realized by the series and parallel of avalanche triodes, and the pulse shaping circuit is made up of the avalanche diode and the two-stage high pass filter with LC. In addition, based on the electric pulse superposition technology and the voltage variation characteristics of dilating pulse transmission along the PC, the improvement of temporal non-uniformity is studied with the optimization of the PC voltage distribution by simultaneously loading the falling edge of the gating pulse and the dilating pulse on the PC. Finally, when the falling edge of the gating pulse is loaded or not loaded on the PC, the temporal uniformity is numerically compared by calculating the dilating ratio of electron beams along the PC, and the temporal uniformity improvement is quantized via the difference percentage between the sampling points.

**Results and Discussions** The picosecond pulse generator [Fig. 2(a)] is designed by the series and parallel of avalanche triodes, the series of avalanche diodes, and the two-stage high pass filter with LC. The gating pulse with an amplitude of −2.59 kV and full width at half maximum of 236 ps is obtained, and its rising and falling edges are 217 ps and 204 ps respectively [Fig. 2 (b)]. Temporal uniformity improvement is analyzed when the falling edge of the gating pulse is loaded or not loaded on the PC and then quantized by the difference percentage between the sampling points [Fig. 4 (d)]. While the falling edge of the gating pulse is not loaded on the PC, the dilating ratio of the electron beam along the PC increases from 11.74 to 39.04, and the difference percentage is 232.5%. When the falling edge is loaded, the dilating ratio rises from 11.28 to 14.23, and the difference percentage is descended to 40.21%. The temporal uniformity of the pulse-dilation framing camera is improved by loading the falling edge of the gating pulse.

**Conclusions** The Marx pulse generator is designed by series and parallel of avalanche triodes. The high-voltage picosecond circuit is designed with avalanche diodes and high pass filters, and the high-voltage picosecond gating pulse is generated. Based on the pulse superposition technology, the temporal uniformity of the pulse dilation framing camera is improved by the falling edge of the gating pulse. The results show that when the PC voltage is −2 kV, the initial width of the electron beam is 5 ps, and the gradient of dilating pulse is 11.9 V/ps, with the transmission of the dilating pulse along the PC, the voltage is changed from −4.48 kV to −2.47 kV, and the dilating ratio of the electron beam grows from 11.74 to 39.04 with the difference percentage of 232.5%. When the falling edge of the gating pulse with the gradient of 12.7 V/ps is simultaneously loaded on the PC, the voltage along the PC is changed from −4.62 kV to −4.97 kV, and the dilating ratio of the electron beam rises from 11.28 to 14.23. The difference percentage is descended to 40.21%, and the temporal uniformity is improved. This study can provide an effective method for improving the temporal non-uniformity of pulse-dilation framing cameras, and a theoretical reference for the development of 10 ps framing cameras with large detection areas.

**Key words** ultrafast optics; ultrafast diagnosis technology; pulse-dilation framing camera; pulse superposition technique; temporal uniformity